International Journal of Biological Macromolecules 141 (2019) 538–544

Contents lists available at ScienceDirect

International Journal of Biological Macromolecules

journal homepage: http://www.elsevier.com/locate/ijbiomac

Rheological, morphological, mechanical, and water-barrier properties of agar/gellan gum/montmorillonite clay composite films

Hansong Lee, Balasubramanian Rukmanikrishnan *, Jaewoong Lee *

Department of Fiber System Engineering, Yeungnam University, South Korea

ARTICLE INFO

Article history:
Received 30 June 2019
Received in revised form 23 August 2019
Accepted 4 September 2019
Available online 5 September 2019

Keywords:
Agar
Gellan gum
MMT clay
Rheological properties
Thermal properties
UV protection
Water barrier properties

ABSTRACT

Agar (A), gellan gum (G) and montmorillonite (M) based ternary nanocomposite films were prepared via the solution-casting method for food packaging applications. The prepared nanocomposites were investigated for the effect of MMT clay on the structure–property relationships by studying the microstructural, rheological, mechanical, thermal, ultraviolet, and water-barrier properties of AG hydrogel composites. The results indicated that the thermal stability ($T_{5\%}$: 119.4–174.7) and tensile strength (29.9–44 MPa) were significantly enhanced in the reinforced MMT nanoclay. The water barrier (1.9–1.7) and contact angle (56.8°–49.4°) were reduced by the incorporation of MMT clay whereas the rheological properties improved. The AGM composite solution exhibited shear thinning behavior and viscosity reduction at a high rate. Additionally, the composites exhibited significantly higher storage and loss modulus at high frequencies. The complex viscosity differed from the shear viscosity and remained higher than the shear viscosity. The nanocomposite structure, molecular interaction, and interaction in the multicomponent were investigated by FT-IR, XRD and SEM analysis. The AG and AGM nanocomposites exhibited a synergistic reinforcement effect. The results of this study might introduce a new route for enhancing the nanocomposites for sustainable materials.

1. Introduction

The consumption of large amounts of non-degradable and non-renewable packaging materials is a significant challenge and presents environmental problems. It is not feasible and wise option to use non-biodegradable polymers for applications which are short-term [1]. Alternatively, biodegradable material in packaging application is a good substitute for non-biodegradable packaging materials [2]. Therefore, to overcome the drawbacks of non-biodegradable materials, biodegradable packaging materials have been developed from natural sources like polysaccharides, proteins, and lipids [3,4]. These natural sources are of plant, animal, and microbial origin [5]. However poor properties, including barrier and mechanical restrict the application of biopolymers in various field when compared to non-biodegradable materials [6–8].

Polysaccharides are widely researched materials for various applications in biomedical field. Agar is made of agarose and agar pectin. It is composed of D-galactose and 3, 6-anhydro-L-galactopyranose along with a heterogeneous combination of smaller molecules [9]. Agar is more stable in different environment such as low-pH and high-temperature. *Sphingomonas paucimobilis* secretes gellan gum which is an exopolysaccharide. It is made up of repeated linear chain of tetrasaccharide units (L-rhamnose, D-glucose, and D-glucuronic acid). With proper cation concentrations, high-acryl gellan gum forms weak gels, and low-acyl gellan gum forms strong gels [10–12].

Biopolymer-based composite films have significant limitations; e.g., they are brittle and have poor water-barrier properties. For overcoming these drawbacks, various methods have been employed. Different nano fillers are used to improve the physical properties of gellan gum and agar-based films. Montmorillonite (MMT) is a commonly used type of clay in biopolymer-based nanocomposites owing to its swelling properties and water holding nature between the platelet layers [13–15]. The clay particles augment physical properties of nanocomposites due to their reinforcing effects. The transparency of MMT based composite is usually maintained with a perfect dispersion of nanosized clay into the polymer matrix [16–19].

Clay is a naturally available mineral and due to its non-toxic nature it is suitable as components in the packaging applications of food, medical and cosmetic industries. Moreover, clay is ecofriendly and inexpensive [1,20]. Many reports are available on clay materials with various natural biopolymers [21–24]. However, as far as we know, there has been no comprehensive study on the effect of MMT nanoclay with gellan gum and agar materials on the rheological and physical and chemical properties of the packaging applications.

To sum up MMT clay's compatibility with gellan gum and agar based films, viability, economic, non-toxic nature and its ability to improve physical properties of composite films makes it an ideal candidate for

* Corresponding authors.
E-mail addresses: rukmibala@gmail.com (B. Rukmanikrishnan), jaewlee@yu.ac.kr (J. Lee).

https://doi.org/10.1016/j.ijbiomac.2019.09.021
0141-8130/

studies. In this experiment, gellan gum, agar, and MMT composites were prepared via a solution-casting method, and the effects of the components on the rheological, mechanical, thermal, and water-vapor permeability (WVP) properties of the composite films were investigated.

2. Materials and methods

2.1. Materials

Agar (viscosity of 40–100 cps at 1.5% in water at 60 °C), gellan gum (low acylation degree), and MMT clay were purchased from Sigma–Aldrich, South Korea. Calcium chloride, glycerin was purchased from Dajang Chemicals, South Korea.

2.2. Preparation of agar/gellan gum/MMT clay composite films

AGM (with 0, 2.5, 5.0, 7.5, and 10 wt% MMT) nanocomposite films were prepared via the solution-casting method. First, agar (1 g) and gellan gum (1 g) were mixed with glycerin (1 g) and calcium chloride (0.5 g). Then, the mixture was added to distilled water (66 ml) with continuous vigorous stirring at 80 °C for 30 min. Additionally, sonication for 60 min at 25 °C dispersed MMT in distilled water (30 ml). Finally, the dispersed MMT was mixed with the agar and gellan gum solution. The solution was stirred for 30 min, and a homogeneous solution was obtained. The solution was cooled to 60 °C, the final film-forming solution was poured uniformly onto a glass plate. All the films were dried at room temperature (25 °C) for 48 h, and then the AGM film was peeled from the glass plate. A series of AG, AGM-2.5, AGM-5, AGM-7.5, and AGM-10 composite films were prepared under similar conditions with different weight % of MMT (0, 2.5, 5, 7.5, and 10 wt%).

2.3. Fourier transform infrared (FT-IR) analysis

FT-IR spectra of the nanocomposites were obtained using a PerkinElmer (Spectrum 100, USA) spectrometer.

2.4. X-ray diffraction (XRD)

XRD patterns of the AGM nanocomposite films were analyzed by X-ray diffractometer (Rigaku D/Max, Japan). XRD spectra were recorded using Cu Kα radiation as an incident X-ray source (40 kV, 200 mA) and scanning speed of 2°/min over a range of $2\theta = 10$ to 80° at room temperature.

2.5. Rheology

The rheological properties of the AGM composites were performed and evaluated using a rheometer (Physica MCR301; Anton Paar, Austria) with parallel-plate geometry (PP25, gap of 1 mm). The analysis was carried out at 25 °C, a dynamic frequency sweep in the range of 0.1–100 1/s at a fixed strain amplitude ($\lambda = 1.0\%$) within a linear viscoelastic region [25,26].

2.6. Differential scanning calorimetry (DSC)

DSC analysis of the AGM nanocomposite films was performed using TA Instruments (USA) at a heating rate of 10 °C/min (25 to 300 °C) under an N_2 atmosphere.

2.7. Thermogravimetric analysis (TGA)

TGA was carried out at a heating rate of 10 °C/min up to 600 °C under N_2 atmosphere using a TA Instruments (SDT Q600 model, USA).

2.8. Optical properties and color analysis

The optical properties of the prepared nanocomposite films were characterized using a Shimadzu (UV-1601, Japan) spectrophotometer in the wavelength range of 200–800 nm. The color values of the nanocomposite films were measured by using a Tristimulus color analyzer (DP-400, Konica Minolta Inc., Japan). The tested samples included brightness and Hunter L*, a*, and b* values. Brightness of the specimen values was examined by the related light ratio of standard (white porcelain reference plate) and tested samples. Hunter color values were tested 10 times for each specimen [27].

2.9. Moisture content (MC)

Mositure content of the AG and AGM composite films were equilibrated at 25 °C and then dried at 100°C for 24 h. The weight difference was calculated using the following equation:

$$\text{Moisture content}(\%) = \frac{W1 - W2}{W1} \times 100$$

Here, W1 and W2 represent the initial and dried weights of the specimen, respectively.

2.10. Contact angle (CA)

CA of AGM films surface was analyzed using a CA analyzer (model OCA 20, GmbH, Germany) on the movable sample stage by placing a drop of water, approximately 10 μL on the surface of the film with micro-syringe.

2.11. Water vapor permeability (WVP)

The WVP of the prepared composite films was determined by the ASTM E-96-95 standard method. The water vapor mass flux (WVTR) in g/m^2 s was determined by using slope of steady-state (linear) portion of the weight change versus time curve. Then, the WVP (g m/m^2 s Pa) of the GXZ film was calculated using the following equation:

$$\text{WVP} = \frac{\text{WVTR} \times L}{\Delta p} \times 100,$$

where L is the mean film thickness (m) and Δp is the partial water vapor pressure difference across the two sides of the film [28].

2.12. Morphology of the films

The morphology of the material after platinum coating was observed using scanning electron microscopy (SEM, Hitachi S-4100) operated at an accelerating voltage of 15 kV.

2.13. Tensile properties

The mechanical properties of the film were studied using universal testing machine (Model 3345, Instron, USA) at a crosshead speed of 300 mm/min using strips according to our previous report [29]. The gauge length was set to 200 mm and the crosshead speed to 300 mm/min.

2.14. Thickness

Digital micrometer (Mituto, Japan) was used to determine the film thickness of the prepared composite films. All the reported values were averages of 5 different locations on each specimen.

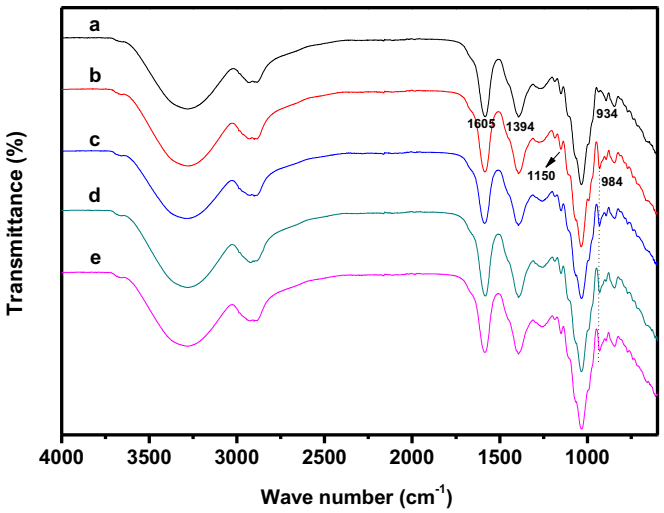

Fig. 1. FT-IR spectra of (a) AG, (b) AGM-2.5, (c) AGM-5, (d) AGM-7.5, and (e) AGM-10.

2.15. Statistical analysis

All the results were subjected to statistical analysis using the SPSS 16 software (USA). The difference among the average values was assessed via Duncan's test. The significance level was $P < 0.05$.

3. Results and discussion

3.1. Ft-IR

The FT-IR spectra of the AG and AGM nanocomposite films are shown in Fig. 1. The broad bands at 2935 and 3287 cm^{-1} were due to the stretching of the hydroxyl (O—H) group and C—H methyl groups present in the agar, gellan gum, and MMT clay materials. The characteristic stretching at 930 cm^{-1} was associated with the CO groups of 3, 6-anhydrogalactose. The peak at 1394 cm^{-1} was attributed to the ester sulfate group of agar [9]. The peak at 1605 and 1394 cm^{-1} in the spectrum of AG composite ascribed to the C═O asymmetric and symmetric stretching vibration of carboxylic acid group which were shifted to 1593 and 1390 cm^{-1} in AGM nanocomposite films. These results indicated strong interaction between AG and MMT matrixes through hydrogen bonds [30,31]. The absorption band at 1150 cm^{-1} is due to the antisymmetric C-O-C stretching of glycoside bands. Fig. 1b shows absorption at 984 cm^{-1}, which is attributed to the stretching vibration of the Si-O-Si group present in the MMT clay [5]. The characteristic results of FT-IR spectra indicated the presence of a molecular interaction between the biopolymer and nanoclay materials in the AG and AGM nanocomposite films.

3.2. Rheological properties

Fig. 2A shows the curves of the shear rate with respect to the shear stress for the AGM composite system. The shear stress increased with the clay concentration. The shear stress significantly increased with the increasing shear rate, owing to the increasing amplitude with an increase in the MMT clay. At a high clay concentration, the AGM network structure was compact owing to the stronger interactions and high viscosity. The hydrodynamic forces on the particles still dominated over their Brownian motion, and the forces were enhanced. Owing to the high interaction, a larger shear stress was needed to break down the network structure [32].

Fig. 2B shows the viscosity of the AGM composites with respect to the shear rate for different MMT clay concentrations. At a shear rate of 1.27 s^{-1}, the shear viscosity of AG composites without MMT was 2.41 Pas which increased to 3.62, 4.72, 9.11 and 8.21 in the presence of 2.5, 5, 7.5 and 10 wt% of MMT respectively. The shear viscosity increased significantly with the increasing MMT content, which was due to the formation of a denser network by the entanglements of the polymer systems at a given shear rate. At higher shear rates, the AGM composites exhibited stronger shear-thinning behavior. This shear-thinning behavior of the AGM composite gel over the whole range of shear rates indicated typical pseudo-plastic behavior. The viscosity of all the nanocomposite films is high at low shear rate. This is due to the high flow resistance and stiffer inner structure of the nanocomposites [33]. When increasing the shear rate, it disrupts the molecular entanglements and flow direction, causing decrease in flow resistance and hence the viscosity [34]. Similar results have been described in previous results on the chitosan derivatives and sodium carboxymethyl cellulose materials [33,35].

The relationships between the complex viscosity (η^*) and storage (G') and loss (G'') moduli of the AGM composite solution and the angular frequency are shown in Fig. 3. Both G' and G'' increased were almost frequency-dependent, and at a high frequency, both G' and G'' increased with the frequency. The values of G' and G'' of AGM nanocomposites at 1.08 (rad/s) are in the range of 11.3–60.29 and 3.84–16.0 Pa respectively. The values of G' were higher than those of G'' for the all AGM composites. Both values increased with the angular frequency, indicating that the elastic property dominated in the viscoelasticity and that a gel-like structure was formed [35]. Moreover, G' and G'' both increased with MMT clay content (from 0 to 10 wt%).

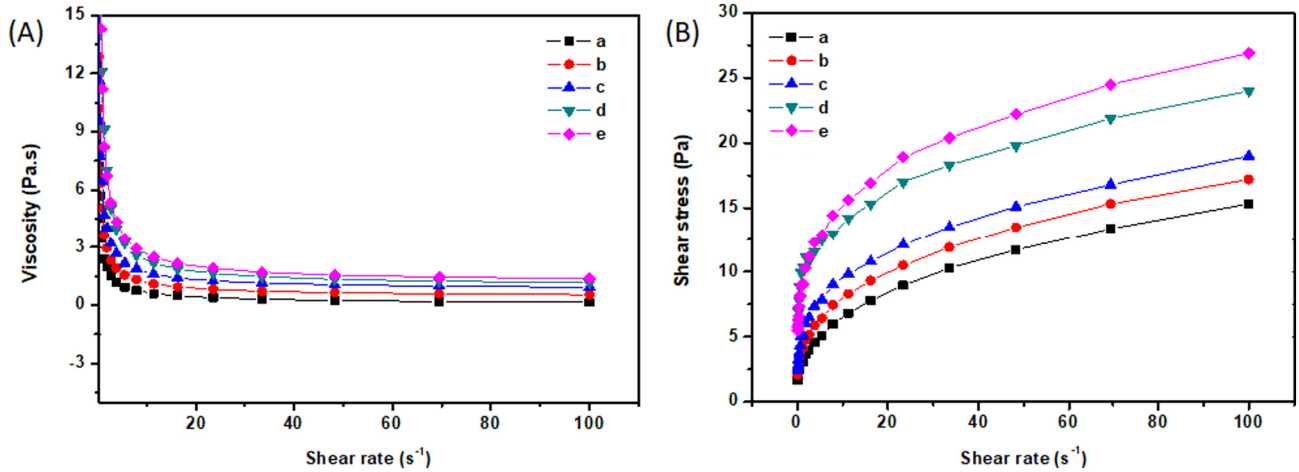

Fig. 2. (A) Shear viscosity and (B) flow curves of (a) AG, (b), AGM-2.5, (c) AGM-5, (d) AGM-7.5, and (e) AGM-10.

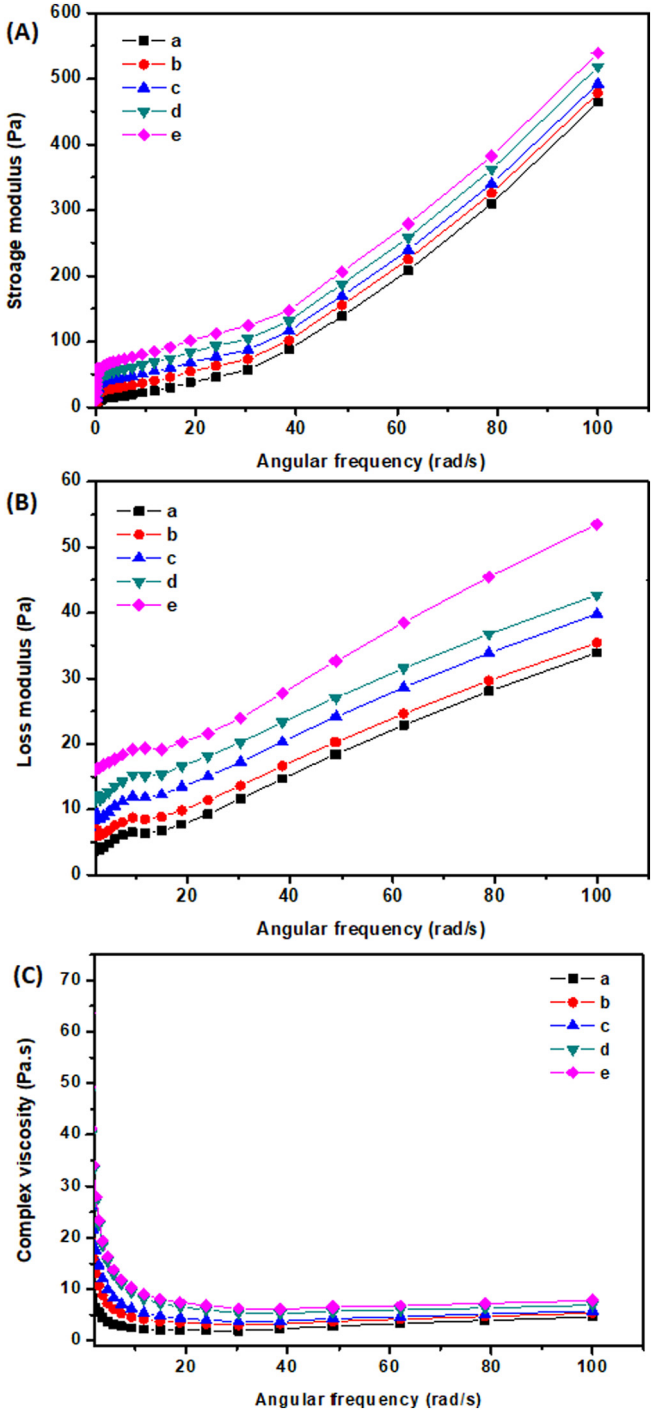

Fig. 3. (A) Storage modulus, (B) loss modulus, and (C) complex viscosity of (a) AG, (b) AGM-2.5, (c) AGM-5, (d) AGM-7.5, and (e) AGM-10.

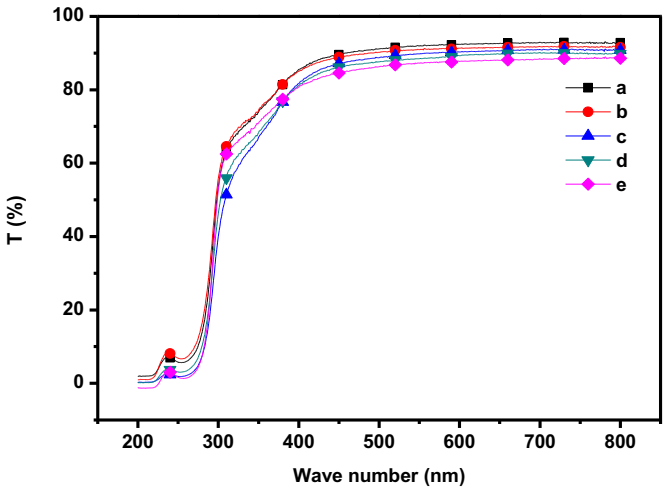

Fig. 4. UV transmittance spectra of (a) AG, (b) AGM-2.5, (c) AGM-5, (d) AGM-7.5, and (e) AGM-10.

The AGM nanocomposites had higher G′, G″, and η* values than the AG composite and exhibited a monotonic increase with an increase in the MMT content. This is because of the confinement or internment of polymer chains within the MMT layers. Complex viscosity (at frequency 1.08 rad/s) of the AG composite was measure to be 11.4 Pa. It was increased to 49.2 Pa for AGM-10. According to the results, at high frequency the moduli of the nanocomposites increased with the MMT content. Furthermore the nanofillers had notable effect on the elastic behavior than the viscous behavior [36]. Fig. 3C shows results of complex viscosity with respect to the angular frequency. The AGM composites exhibited pseudo-Newtonian behavior and shear thinning with an increase in the frequency. MMT incorporation increased the complex viscosity of AG composites. The flow restriction of the composites leads to a higher viscosity of the AGM nanocomposites. The AGM chain structure significantly governed the rheological properties and the processability of the polymer. In general, at a low frequency, the interaction between AG and MMT overcame the applied shear. However, at a higher frequency, the interfacial bonding between AG and MMT could not resist the external shear. Therefore the overall results of AGM nanocomposites were similar and comparable to the report present in the literature [32,36–38].

3.3. Ultraviolet (UV)

Table 1 and Fig. 4 show the optical properties of the AGM nanocomposite films. The transparency of the nanocomposite films decreased with addition of MMT nanoclay particles. The AG and AGM-10 exhibited similar transmittance at 800 nm. The UV transmittance of the AG and AGM nanocomposite films was in the range of 93.2%–88.4% at 600 nm. The results indicate uniform dispersion with marked compatibility

Table 1
UV-transmittance, thickness and color values of the AG and AMG nanocomposite films.

Sample	Thickness (mm)	Transmittance (%) at 600 nm	Hunter color scale values[#]		
			Lightless (L*)	Redness (a*)	Yellowness (b*)
AG	0.10 ± 0.01	93.2 ± 0.2^{a}	84.51 ± 0.38^{a}	−0.22 ± 0.04^{a}	1.67 ± 0.17^{e}
AGM-2.5	0.09 ± 0.01	92.0 ± 0.3^{a}	83.91 ± 0.41^{b}	−0.30 ± 0.02^{b}	2.89 ± 0.23^{d}
AGM-5.0	0.12 ± 0.01	91.1 ± 0.2^{ab}	83.24 ± 0.32^{c}	−0.41 ± 0.03^{c}	3.85 ± 0.20^{c}
AGM-7.5	0.11 ± 0.01	89.6 ± 0.1^{b}	82.97 ± 0.43^{c}	−0.56 ± 0.02^{d}	5.17 ± 0.10^{b}
AGM-10	0.11 ± 0.00	88.4 ± 0.2^{b}	82.75 ± 0.14^{cd}	−0.64 ± 0.04^{e}	6.16 ± 0.34^{a}

*Each value is the mean of replicates with the standard deviation. Any two means in the same superscript letter in the same column indicate that they are not significantly ($p^{\circ}0.05$) different.

[#] L* (0: black, 100: white), a* (−: green, +: red), b* (−: blue, +: yellow). Each value represents mean ± standard deviation (SD) of three independent.

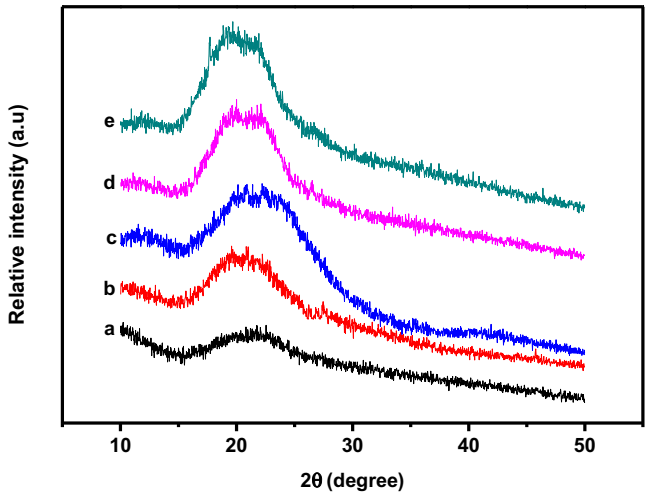

Fig. 5. X-ray diffractogram of (a) AG, (b) AGM-2.5, (c) AGM-5, (d) AGM-7.5, and (e) AGM-10.

among the agar, gellan gum, and MMT nanoclay. The color values of the all the composite films are summarized in Table 1. AG and AGM nanocomposite films are transparent. Addition of MMT nanoclay reduced the value of chromatic axes L*and a* and increased the value of b* axis. However, the changes in the color parameters were not significantly different.

3.4. XRD

Miscibility of the components in a polymer matrix is characterized by XRD method. XRD analysis was performed on the AG and AGM nanocomposite films (Fig. 5). None of the XRD patterns of the nanocomposite films exhibited sharp peaks. This indicates that the nanocomposite films were amorphous in nature and had a noncrystalline structure. No new peaks were detected after the addition of MMT. This suggests that the nanoclay was substantially exfoliated and that polymer chains were incorporated between the silicate layers resulting in the exfoliated nanomorphology of the AGM matrix [22]. The outcomes indicate that addition of MMT is helpful in obtaining exfoliated nanocomposite films. The two broad peaks around 20° appears as single broad peakwith increase in the MMT concentration [5,11]. The changes in the XRD patterns revealed that the presence of intermolecular H bonding interaction between the nanoclay and polymers matrixes. The ultrasonication of a MMT clay dispersion are good for developing a high degree of intercalation [39].

3.5. SEM

SEM images of AG composite films with MMT nanoclay are shown in Fig. 6. The surfaces of the AG and AGM nanocomposites were smooth and homogeneous. The weight percentages of the nanoclay particles significantly affected their homogenous dispensability in the film matrix. Incorporation of a large amount (AGM- 10) of MMT nanoclay to the AG matrix increased the surface roughness. This may be due to the tendency of the nanoclay particles to aggregate at higher concentration resulting in non-uniform dispersion in the polymer matrix unlike in AGM-2.5, 5, 7.5 wt%. This agglomeration of MMT clay in AGM-10, resulted in a reduced tensile strength (TS) of the nanocomposites. This result agrees with the mechanical properties of the AGM nanocomposites.

3.6. WVP

Permeability depends on the solubility and diffusivity of water in the polymer matrix [5]. The WVP of the AG and AGM composite films is presented in Table 1. The WVP of the AG composite films was 1.9, and it decreased to 1.70 for AGM-10 (as the nanoclay content increased). The incorporation of MMT nanoclay particles significantly influenced the WVP of the nanocomposites. Similar results for nanoclay have been frequently observed with various biopolymers [21,33]. However, the WVP of AGM-5 was not improved compared to that of AGM-4 nanocomposite films. This is due to the tendency of the nanoclay particles to aggregate at higher concentration, some as noticed in the SEM images.

3.7. Contact angle and moisture content

Contact angle (CA) analysis is an important parameter to investigate the wettability of the packaging composite materials. The CA depends on the cohesive and adhesive molecular forces within the water and surface of the film. The CA of the AG film was 56.8°, and it decreased to 49.4° as the nanoclay content increased. This is mainly due to the

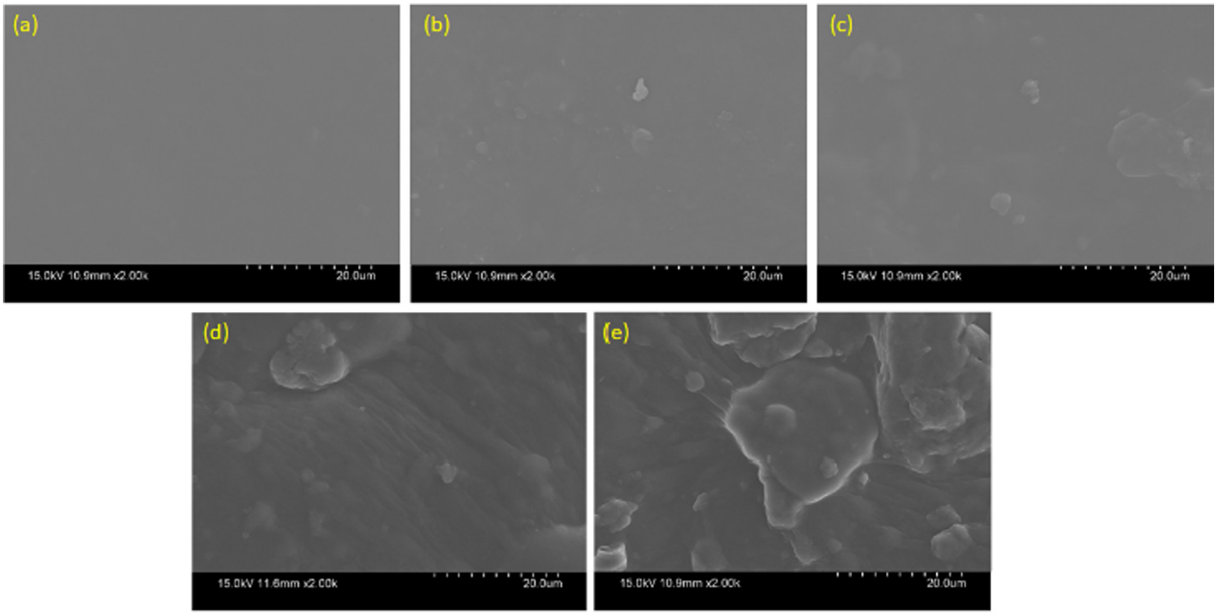

Fig. 6. SEM images of (a) AG, (b) AGM-2.5, (c) AGM-5, (d) AGM-7.5, and (e) AGM-10.

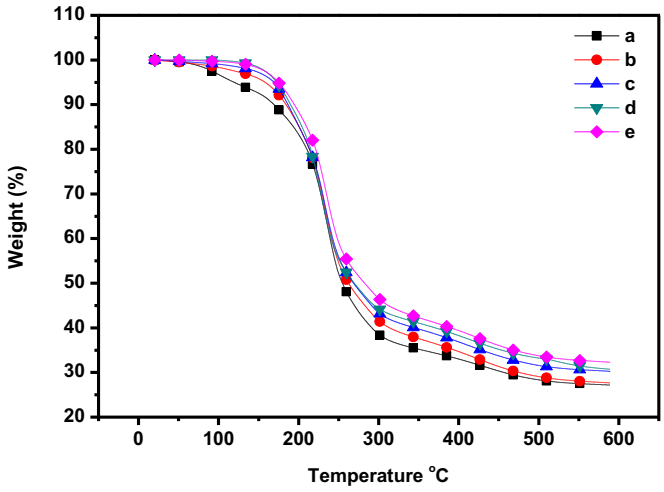

Fig. 7. TGA results for (a) AG, (b) AGM-2.5, (c) AGM-5, (d) AGM-7.5, and (e) AGM-10.

hydrophilic nature of the MMT clay particles. Moisture content of the AG and AGM nanocomposites decreased significantly (from 21.3% to 14.1%) with the incorporation of MMT nanoclay. These results suggest that the MMT nanoclay reduced the moisture sensitivity of the AGM nanocomposites.

3.8. TGA

The thermal stability of the AG and AGM nanocomposites was assessed via TGA. Fig. 7 and Table 2 present the char yield and 5% ($T_{5\%}$) and 10% ($T_{10\%}$) gravimetric loss for the AG and AGM nanocomposites. The $T_{5\%}$ and $T_{10\%}$ weight loss of the nanocomposite films increased from 119.4 to 174.7 °C and 169.1-194.5 °C respectively. The weight loss of the AG composite shifted toward a higher temperature when MMT was incorporated into the polymer matrix. The maximum weight loss rate was closely related to the thermal characteristic of the polymer matrix. Owing to the addition of MMT clay, AGM-10 exhibited the highest weight-loss temperature ($T_{5\%}$ and $T_{10\%}$). This value increased significantly with the addition of MMT clay [9]. The residual char yield of the AG at 600 °C was 27.2%, and it increased to 32.3% in the AGM nanocomposite film. The residual weight percentage of all the AGM nanocomposites at 600 °C is higher than the AG composite owing to the presence of strong interaction between agar, gellan gum and MMT clay materials [5,17,40]. To compare with previous reports, the prepared AG composite has a better char yield than neat agar composites [7,9,10]. This improvement of resistance against temperature may be due to strengthening of the AG rigidity caused by the interaction between the components which reduces the molecular mobility [12]. The increased thermal stability of the AGM nanoclay film in all the stages indicates a homogenous dispersion of MMT in the AG matrix. The clay functioned as a heat barrier, enhancing the thermal stability of the composite films (Table 3).

Table 3
Thermal properties of the AG and AMG nanocomposite films.

Sample	TGA			DSC		
	$T_{5\%}$	$T_{10\%}$	CY (%)	T_g (°C)	T_c (°C)	T_m (°C)
AG	119.4	169.1	27.2	70.2 ± 0.4^{e}	157.9 ± 0.7^{d}	198.4 ± 0.3^{c}
AGM-2.5	158.1	184.3	27.7	71.6 ± 0.6^{d}	161.5 ± 0.7^{c}	206.6 ± 0.2^{b}
AGM-5.0	169.5	186.6	30.2	73.4 ± 0.5^{c}	163.3 ± 0.5^{bc}	208.4 ± 0.4^{b}
AGM-7.5	172.6	189.8	30.9	75.3 ± 0.4^{b}	164.0 ± 0.6^{b}	213.9 ± 0.5^{a}
AGM-10	174.7	194.5	32.3	77.1 ± 0.8^{a}	166.9 ± 0.7^{a}	214.2 ± 0.5^{a}

*Each value is the mean of replicates with the standard deviation. Any two means in the same superscript letter in the same column indicate that they are not significantly (p˃0.05) different.

3.9. DSC

DSC analysis of the AG and AGM nanocomposites revealed the glass transition temperature (T_g), crystalline temperature (T_c) and melting temperature (T_m), providing valuable understating of the structural arrangements and interactions between the polymers and MMT nanoclay. The nanocomposite films showed statistically notable differences in the T_g values (p ˂ 0.05). The T_g and T_c values of the AG and AGM nanocomposite films were in the range of 70.2–77.1 and 157.9–166.9 °C respectively. As the MMT concentration increased from 0 to 10 wt%, T_g value increased steadily. The increase in T_g with the addition of MMT nanoclay is attributed to fact that there was no plasticization effect dispersed in the polymer matrix [16]. Additionally, the incorporation of MMT raised the melting temperature of the nanocomposite films. The values were not statistically significant.

3.10. Mechanical properties

Tensile strength (TS) and elongation at break (EB) were the mechanical properties determined for the AG and AGM nanocomposite films. The observed values are presented in Table 2. The mechanical properties were significantly influenced by the incorporation of nanoclay with different weight percentages. The TS of the AG composite increased from 29.9 to 44 MPa with the addition of 0–10 wt% MMT nanoclay. The interaction between the clays large surface area and the polymer matrix facilitated the formation of constrained regions of high rigidity, transferring the stress to the reinforcement phase, and therefore enhancing the TS of the nanocomposites [6,41].

The EB of the AG and AGM nanocomposite films decreased from 29.5% to 19.9% with an increase in the MMT nanoclay content0–10 wt %. The clay–polymer interaction prevented the easy sliding of polymer chains against each other, reducing the EB of the nanocomposites. These results agree well with previous works [4,9]. Mechanical strength of the nanocomposites in an intercalated system increased with a higher clay content. The AG and AGM nanocomposites films exhibited improved water-barrier and mechanical properties. These nanocompos-

Table 2
Water vapor permeability, contact angle, moisture content and mechanical properties of the AG and AMG nanocomposite films.

Sample	Water vapor permeability ($\times 10^{-9}$ g/m^2 Pas)	Water contact angle (°)	Moisture content (%)	Tensile strength (MPa)	Elongation at break (%)
AG	1.90 ± 0.18^{a}	56.8 ± 1.6^{a}	21.3 ± 0.4^{a}	29.9 ± 1.2^{d}	29.5 ± 0.9^{a}
AGM-2.5	1.81 ± 0.15^{b}	56.6 ± 1.1^{a}	19.7 ± 0.6^{b}	35.3 ± 1.3^{c}	24.1 ± 0.8^{b}
AGM-5.0	1.74 ± 0.12^{c}	54.6 ± 1.7^{b}	17.5 ± 0.6^{c}	39.4 ± 0.8^{b}	22.4 ± 1.1^{bc}
AGM-7.5	1.66 ± 0.14^{d}	54.4 ± 2.2^{b}	16.1 ± 0.5^{d}	43.2 ± 0.9^{a}	20.7 ± 0.8^{c}
AGM-10	1.70 ± 0.11^{d}	49.4 ± 1.4^{c}	14.1 ± 0.6^{e}	44.0 ± 1.4^{a}	19.9 ± 0.8^{c}

*Each value is the mean of replicates with the standard deviation. Any two means in the same superscript letter in the same column indicate that they are not significantly (p˃0.05) different.

ites have great potential as inexpensive, biodegradable alternatives to conventional plastics for flexible packaging applications.

4. Conclusions

Different weight percentages of MMT clay were used to prepare agar and gellan gum based nanocomposite films. FT-IR characterization indicated that the agar and gellan gum were miscible and that an intermolecular interaction occurred. Rheology analysis revealed that the MMT improved the properties of the AG solution. The composites exhibited significantly high storage and loss modulus at a high frequency as the clay content increased. The AGM exhibited shear-thinning behavior over the entire applied frequency range. The complex viscosity slightly differed from the shear viscosity of the AGM composites. The SEM images showed different patterns of microstructure. With the addition of MMT (10 wt%), there was an increase in the tensile strength from 29.9 to 44.0 MPa which improved by 47.1% when compared to neat AG composite film. The AGM nanocomposite films exhibited high thermal stability ($T_{5\%}$: 119.4–174.7 °C) which improved by 46.3% when compared to neat AG composite film. The addition of MMT clay decreased both the WVP and moisture content values of the nanocomposite films. Therefore, the nanocomposites have great potential as an inexpensive and biodegradable alternative to conventional plastics for flexible packaging applications.

Declaration of competing interest

There are no conflicts to declare.

Acknowledgements

This work was aided by the Technology Innovation Program (or industrial strategic technology development program, 10076409, establishment of solution for optical/light design/dynamic concept hybrid 2D/3D thermoplastic prepreg for design performance) funded by the Ministry of Trade, Industry and Energy (MOTIE Korea).

References

[1] A.C. Souza, R. Benze, E.S. Ferrão, C. Ditchfield, A.C.V. Coelho, C.C. Tadini, Cassava starch biodegradable films: influence of glycerol and clay nanoparticles content on tensile and barrier properties and glass transition temperature, LWT Food Sci. Technol. 46 (2012) 110–117.
[2] Huafeng Tiana, Kai Wang, Di Liu, Jiaan Yan, Aimin Xiang, A. Varada Rajulu, Enhanced mechanical and thermal properties of poly (vinyl alcohol)/corn starch blends by nanoclay intercalation, Int. J. Biol. Macromol. 101 (2017) 314–320.
[3] Chaturbhuj K. Saurabh, Sumit Gupta, Jitendra Bahadur, S. Mazumder, Prasad S. Variyar, Arun Sharma, Mechanical and barrier properties of guar gum based nanocomposite films, Carbohydr. Polym. 124 (2015) 77–84.
[4] Mehdi Alboofetileh, Masoud Rezaei, Hedayat Hosseini, Mehdi Abdollahi, Antimicrobial activity of alginate/clay nanocomposite films enriched with essential oils against three common foodborne pathogens, Food Control 36 (2014) 1–7.
[5] Aníbal M. Slavutsky, María A. Bertuzzi, Margarita Armada, María G. García, Nelio A. Ochoa, Preparation and characterization of montmorillonite/brea gum nanocomposites films, Food Hydrocoll. 35 (2014) 270–278.
[6] Xiaozhi Tang, Sajid Alavi, Structure and physical properties of starch/poly vinyl alcohol/laponite RD nanocomposite films, J. Agric. Food Chem. 60 (2012) 1954–1962.
[7] Shiv Shankar, Jong-Whan Rhim, Preparation and characterization of agar/lignin/silver nanoparticles composite films with ultraviolet light barrier and antibacterial properties, Food Hydrocoll. 71 (2017) 76–84.
[8] Saliha Memiş, Fatih Tornuk, Fatih Bozkurt, M. Zeki Durak, Production and characterization of a new biodegradable fenugreek seed gum based active nanocomposite film reinforced with nanoclays, Int. J. Biol. Macromol. 103 (2017) 669–675.
[9] Liang Wang, David A. Schiraldi, Miguel Sánchez-Soto, Foam like xanthan gum/clay aerogel composites and tailoring properties by blending with agar, Ind. Eng. Chem. Res. 53 (2014) 7680–7687.
[10] Maria A. Bonifacio, Piergiorgio Gentile, Ana M. Ferreira, Stefania Cometa, Elvira De Giglio, Insight into halloysite nanotubes-load gellan gum hydrogels for soft tissue engineering applications, Carbohydr. Polym. 163 (2017) 280–291.
[11] X. Xu, B. Li, J.F. Kennedy, B.J. Xie, M. Huang, Characterization of konjac glucomannan–gellan gum blend films and their suitability for release of nisin incorporated therein, Carbohydr. Polym. 70 (2007) 192–197.
[12] Rukmanikrishnan Balasubramanian, Sam Soo Kim, Jaewoong Lee, Novel synergistic transparent -carrageenan/k xanthan gum/gellan gum hydrogel film: mechanical, thermal and water barrier properties, Int. J. Biol. Macromol. 118 (2018) 561–568.
[13] C.H. Zhou, Z.F. Shen, L.H. Liu, S.M. Liu, Preparation and functionality of clay-containing films, J. Mater. Chem. 21 (2011) 15132–15153.
[14] H.L. Tyan, Y.C. Liu, K.Hw. Wei, Thermally and mechanically enhanced clay/polyimide nanocomposite via reactive organoclay, Chem. Mater. 11 (1999) 1942–1947.
[15] K.S. Triantafyllidis, P.C. LeBaron, I. Park, T.J. Pinnavaia, Epoxy-clay fabric film composites with unprecedented oxygen-barrier properties, Chem. Mater. 18 (2006) 4393–4398.
[16] Viviane Machado Azevedo, Eric Keven Silva, Camila Ferreira Gonçalves Pereira, Joyce Maria Gomes da Costa, Soraia Vilela Borges, Whey protein isolate biodegradable films: influence of the citric acid and montmorillonite clay nanoparticles on the physical properties, Food Hydrocoll. 43 (2015) 252–258.
[17] Saffawati Syazwani Mohd, Mohd Aidil Adhha Abdullah, Khairul Anuar Mat Amin, Gellan gum/clay hydrogels for tissue engineering application: mechanical, thermal behavior, cell viability, and antibacterial properties, J. Bioact. Compat. Polym. 31 (2016) 648–666.
[18] Sirajo Abubakar Zauro, B. Vishalakshi, Amphoteric gellan gum-based terpolymer–montmorillonite composite: synthesis, swelling, and dye adsorption studies, Int. J. Ind. Chem. 8 (2017) 345–362.
[19] A.A. Sapalidis, F.K. Katsaros, Th.A. Steriotis, N.K. Kanellopoulos, Properties of poly (vinyl alcohol)—bentonite clay nanocomposite films in relation to polymer–clay interactions, J. Appl. Polym. Sci. 123 (2012) 1812–1821.
[20] Sibel Tunç, Osman Duman, Preparation and characterization of biodegradable methyl cellulose/montmorillonite nanocomposite films, Appl. Clay Sci. 48 (2010) 414–424.
[21] Mehdi Alboofetileh, Masoud Rezaei, Hedayat Hosseini, Mehdi Abdollahi, Effect of montmorillonite clay and biopolymer concentration on the physical and mechanical properties of alginate nanocomposite films, J. Food Eng. 117 (2013) 26–33.
[22] Younes Zahedia, Bahram Fathi-Achachlouei, Ali Reza Yousefi, Physical and mechanical properties of hybrid montmorillonite/zinc oxide reinforced carboxymethyl cellulose nano composites, Int. J. Biol. Macromol. 108 (2018) 863–873.
[23] Hadi Almasi, Babak Ghanbarzadeh, Ali A. Entezami, Physicochemical properties of starch–CMC–nanoclay biodegradable films, Int. J. Biol. Macromol. 46 (2010) 1–5.
[24] Joanna Dziadkowiec, Rola Mansa, Ana Quintela, Fernando Rocha, Christian Detellier, Preparation, characterization and application in controlled release of Ibuprofen-loaded Guar Gum/Montmorillonite Bionanocomposites, Appl. Clay Sci. 135 (2017) 52–63.
[25] Anuj Kumar, Sun Mi Zo, Joon Ho Kim, Seong-Cheol Kim, Sung Soo Han, Enhanced physical, mechanical, and cytocompatibility behavior of polyelectrolyte complex hydrogels by reinforcing halloysite nanotubes and graphene oxide, Compos. Sci. Technol. 175 (2019) 35–45.
[26] M.J. Ramazani-Harandi, M.J. Zohuriaan-Mehr, A.A. Yousefi, A. Ershad-Langroudi, K. Kabiri, Rheological determination of the swollen gel strength of superabsorbent polymer hydrogels, Polym. Test. 25 (2006) 470–474.
[27] J.S. Lee, R. Srinivasan, I.G. Jo, Y.S. Kwon, B. Ashutosh, Y.S. Oh, O.J. Kwon, M. Kim, Comparative study of the physicochemical, nutritional, and antioxidant properties of some commercial refined and non-centrifugal sugars, Food Res. Int. 109 (2018) 614–625.
[28] A. Gennadios, C.L. Weller, C.H. Gooding, Measurement errors in water vapor permeability of highly permeable, hydrophilic edible films, J. Food Eng. 21 (1994) 395–409.
[29] R. Balasubramanian, S.S. Kim, J. Lee, J. Lee, J. Effect of TiO2 on highly elastic, stretchable UV protective nanocomposite films formed by using a combination of k-Carrageenan, xanthan gum and gellan gum, Int. J. Biol. Macromol. 123 (2019) 1020–1027.
[30] X.N. Zhang, Y.J. Wang, S. Sun, L. Hou, P. Wu, Z.L. Wu, Q. Zheng, A tough and stiff hydrogel with tunable water content and mechanical properties based on the synergistic effect of hydrogen bonding and hydrophobic interaction, Macromolecules 51 (2018) 8136–8146.
[31] B.D. Kevadiya, S. Rajkumar, H.C. Bajaj, S.S. Chettiar, K. Gosai, H. Brahmbhatt, A.S. Bhatt, Y.K. Barvaliya, G.S. Dave, R.K. Kothari, Biodegradable gelatin–ciprofloxacin–montmorillonite composite hydrogels for controlled drug release and wound dressing application, Colloids Surf. B: Biointerfaces 122 (2014) 175–183.
[32] Ying Liu, Liyan Liu, Yang Wang, Guorui Zhu, Wei Tan, The rheological behavior of graphite oxide/cationic polyacrylamide suspensions, RSC Adv. 6 (2016) 102938–102946.
[33] Beibei Wang, Xiaodeng Yang, Congde Qiao, Tianduo Li, Chunlin Xu, Effects of chitosan quaternary ammonium salt on the physicochemical properties of sodium carboxymethyl cellulose-based films, Carbohydr. Polym. 184 (2018) 37–46.
[34] Tae H. Kim, Lee W. Jang, Dong C. Lee, Hyoung J. Choi, Myung S. Jhon, Synthesis and rheology of intercalated polystyrene/Na+-montmorillonite nanocomposites, Macromol. Rapid Commun. 23 (2002) 191–195.
[35] Beibei Wang, Congde Qiao, Xinyue Gao, Xiaodeng Yang, Yan Li, Tianduo Li, Rheological properties of *N*-[(2-hydroxyl)-propyl-3-trimethyl ammonium] chitosan chloride, Carbohydr. Polym. 171 (2017) 50–58.
[36] Mohagheghian Majid, Ebadi-Dehaghani Hassan, Ashouri Davoud, Mousavian Saman, A study on the effect of nano-ZnO on rheological and dynamic mechanical properties of polypropylene: experiments and models, Compos. Part B 42 (2011) 2038–2046.
[37] J.L. Xu, J.C. Zhang, Y. Liu, H.J. Sun, J.H. Wang, Rheological properties of a polysaccharide from floral mushrooms cultivated in Huangshan Mountain, Carbohydr. Polym. 139 (2016) 43–49.
[38] M. Aguilar-Zárate, B.A. Macias-Rodriguez, J.F. Toro-Vazquez, A.G. Marangoni, Engineering rheological properties of edible oleogels with ethylcellulose and lecithin, Carbohydr. Polym. 205 (2019) 98–105.
[39] J.W. Rhim, Effect of clay contents on mechanical and water vapor barrier properties of agar-based nanocomposite films, Carbohydr. Polym. 86 (2011) 691–699.
[40] Y. Huang, J. Lu, C. Xiao, Thermal and mechanical properties of cationic guar gum/poly(acrylic acid) hydrogel membranes, Polym. Degrad. Stab. 92 (2007) 1072–1081.
[41] J.H. Lee, D. Jung, C.E. Hong, K.Y. Rhee, S.G. Advani, Properties of polyethylene-layered silicate nanocomposites prepared by melt intercalation with a PP-g-MA compatibilizer, Compos. Sci. Technol. 65 (2005) 1996–2002.